

## Synthetic Spin-Orbit Coupling in an Optical Lattice Clock

Michael L. Wall,<sup>1,2,\*</sup> Andrew P. Koller,<sup>1,2,3</sup> Shuming Li,<sup>1,3</sup> Xibo Zhang,<sup>1,3,†</sup>  
Nigel R. Cooper,<sup>4</sup> Jun Ye,<sup>1,3</sup> and Ana Maria Rey<sup>1,2,3</sup>

<sup>1</sup>JILA, NIST and University of Colorado, 440 UCB, Boulder, Colorado 80309, USA

<sup>2</sup>Center for Theory of Quantum Matter, University of Colorado, Boulder, Colorado 80309, USA

<sup>3</sup>Department of Physics, University of Colorado, 440 UCB, Boulder, Colorado 80309, USA

<sup>4</sup>T.C.M. Group, Cavendish Laboratory, J.J. Thomson Avenue, Cambridge CB3 0HE, United Kingdom

(Received 23 September 2015; published 22 January 2016)

We propose the use of optical lattice clocks operated with fermionic alkaline-earth atoms to study spin-orbit coupling (SOC) in interacting many-body systems. The SOC emerges naturally during the clock interrogation, when atoms are allowed to tunnel and accumulate a phase set by the ratio of the “magic” lattice wavelength to the clock transition wavelength. We demonstrate how standard protocols such as Rabi and Ramsey spectroscopy that take advantage of the sub-Hertz resolution of state-of-the-art clock lasers can perform momentum-resolved band tomography and determine SOC-induced *s*-wave collisions in nuclear-spin-polarized fermions. With the use of a second counterpropagating clock beam, we propose a method for engineering controlled atomic transport and study how it is modified by *p*- and *s*-wave interactions. The proposed spectroscopic probes provide clean and well-resolved signatures at current clock operating temperatures.

DOI: 10.1103/PhysRevLett.116.035301

The recent implementation of synthetic gauge fields and spin-orbit coupling (SOC) in neutral atomic gases [1–7] is a groundbreaking step towards using these fully controllable systems to synthesize and probe novel topological states of matter. To date, optical Raman transitions have been used to couple different internal (e.g., hyperfine) states while transferring net momentum to the atoms. However, in alkali atoms Raman-induced spin flips inevitably suffer from heating mechanisms associated with spontaneous emission. While this issue has not yet been an impediment for the investigation of noninteracting processes or mean field effects [4,5], it could limit the ability to observe interacting many-body phenomena that manifest at longer time scales. Finding alternative, more resilient methods for generating synthetic SOC—and for probing its interplay with interactions—is thus highly desirable.

To reduce heating, the use of atoms with richer internal structure such as alkaline-earth atoms (AEAs) [3,7] or lanthanide atoms such as Dy and Er [8] has been suggested. In addition to long-lived electronic states AEAs also offer accessible electronic state-dependent trapping potentials with applications that range from the generation of synthetic gauge fields [9] and particle number fractionalization [10,11] to quantum information processing [12,13]. Most of the existing proposals require complicated experimental setups including laser-assisted tunneling and rectification protocols or have been targeted to study the noninteracting regime [7]. Here, we demonstrate that SOC emerges naturally in cold AEA optical lattice clocks (OLCs) [14] that use a “magic” (state independent) lattice. This is because the clock laser imprints a phase that varies significantly from one lattice site to the next as it drives an ultranarrow optical transition. Our implementation (1) uses a direct transition to a long-lived

electronic clock state with a natural lifetime  $\gtrsim 10^2$  s [15] (and thus heating from spontaneous emission is negligible), (2) takes advantage of the sub-Hz resolution of clock lasers [16–19], and (3) accesses the regime where the interaction energy per particle,  $U$ , is weak compared to the characteristic trapping energies [20–25] but comparable to SOC scales determined by  $J$ , the tunneling, and  $\Omega$ , the clock Rabi frequency. This regime allows us to investigate the interplay of interactions and SOC, to carry out controllable analytic calculations and make concrete predictions, and to devise feasible interaction sensitive probing protocols accessible and testable in current experiments.

In the first protocol, we demonstrate that momentum-resolved tomography of chiral band structures can be performed using Rabi spectroscopy in the parameter regime  $J \sim \Omega \gg U$ . In the second protocol we show that the modification of collisional properties by SOC [26,27] is manifest in standard Ramsey spectroscopy, focusing on the parameter regime  $J \gtrsim U$ . In the final protocol, controlled and spatially resolved atomic transport [28–35] is induced by an additional counterpropagating clock beam that exhibits a controllable phase difference with respect to the original probe beam. Interaction effects beyond mean field are shown to modify the dynamics in the parameter regime  $\Omega \gg J \sim U$ . Inelastic collisions in the excited state impose limitations in the probing time [24,25,36,37]; however, they can be dynamically accounted for during clock interrogation, as demonstrated in Refs. [20,24]. We also show that losses can be used as a resource for state preparation and read-out.

Current OLCs interrogate the  ${}^1S_0(g)$ - ${}^3P_0(e)$  transition of ensembles of thousands of nuclear-spin-polarized fermionic AEAs trapped in a deep 1D optical lattice that splits the gas in an array of 2D pancakes [14] (see Fig. 1). The

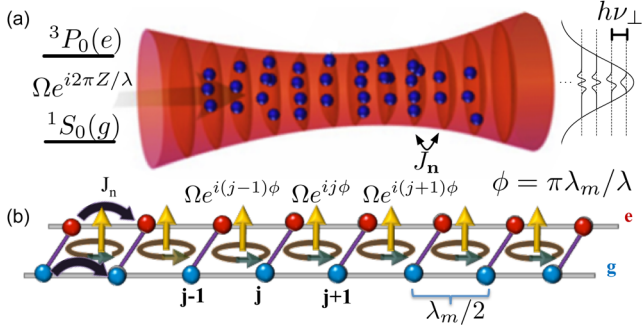


FIG. 1. (a) A clock laser along the  $Z$  direction of wavelength  $\lambda$  and Rabi frequency  $\Omega$  interrogates the  $^1S_0(g)$ - $^3P_0(e)$  transition in fermionic alkaline-earth atoms trapped in an optical lattice with magic wavelength  $\lambda_m$ . The transverse confinement is provided by Gaussian curvature of the lattice beams with harmonic frequency  $h\nu_\perp$ . Many transverse modes  $\mathbf{n}$  are populated at current operating temperatures. (b) The phase difference  $\phi$  between adjacent sites  $j$  and  $(j+1)$  induces SOC when atoms can tunnel with mode-dependent tunnel coupling  $J_{\mathbf{n}}$ , realizing a synthetic two-leg ladder with flux  $\phi$  per plaquette.

lattice potential uses the magic wavelength,  $\lambda_m$ , to generate identical trapping conditions for the two states. At current operating temperatures,  $T \sim \mu\text{K}$  [20], the population of higher axial bands is negligible ( $\lesssim 5\%$ ). On the other hand, along the transverse directions, where the confinement is provided wholly by the Gaussian curvature of the optical lattice beams, modes are thermally populated with an average number of mode quanta  $\langle n \rangle \sim 50$ . To generate SOC, coherent tunneling between the lattice sites is required. Our proposal is to superimpose a running-wave beam on the lattice potential:

$$V_{\text{ext}}(\mathbf{R}) = -\exp\left(-\frac{2R^2}{w_0^2}\right) \left[ V_{\text{const}} + V \cos^2\left(\frac{2\pi Z}{\lambda_m}\right) \right]; \quad (1)$$

this increases the transverse confinement without significantly affecting the axial motion [38]. Here,  $w_0$  is the beam waist,  $R$  the transverse radial coordinate,  $Z$  the axial coordinate,  $V$  the axial lattice corrugation, and  $V_{\text{const}}$  the running-wave induced potential. By increasing  $V_{\text{const}}$  as  $V$  is lowered, the transverse confinement frequency  $\nu_\perp \sim \sqrt{(1/m\pi^2 w_0^2)(V_{\text{const}} + V)}$ , with  $m$  being the atom mass, is kept constant, while the tunneling rate along the axial direction increases.

Since  $V_{\text{ext}}(\mathbf{R})$  is discretely translationally invariant along the axial direction, atoms trapped in the lowest axial lattice band are governed by the Hamiltonian  $\hat{H}^0 = \sum_{\mathbf{n}} \hat{H}_{\mathbf{n}}^0$  [39]:

$$\hat{H}_{\mathbf{n}}^0 = \sum_{q,\alpha} E_{\alpha,\mathbf{n},q} \hat{n}_{\alpha,\mathbf{n},q} - \sum_q \left[ \frac{\Omega_{\mathbf{n}}}{2} \hat{a}_{+,q+\phi}^\dagger \hat{a}_{-,q,q} + \text{H.c.} \right]. \quad (2)$$

Throughout,  $q = \tilde{q}a$  is the dimensionless product of axial quasimomentum  $\tilde{q}$  and the lattice spacing  $a = \lambda_m/2$ ,  $\hat{a}_{\alpha,\mathbf{n},q}$  annihilates a fermion in the two-dimensional transverse mode  $\mathbf{n}$ , quasimomentum  $q$ , state  $\alpha = \pm$  (for  $e$  and  $g$ ),

and  $\hat{n}_{\alpha,\mathbf{n},q} = \hat{a}_{\alpha,\mathbf{n},q}^\dagger \hat{a}_{\alpha,\mathbf{n},q}$ . The energy  $E_{\alpha,\mathbf{n},q}(q) = \alpha(\delta/2) + \bar{E}_{\mathbf{n}} - 2J_{\mathbf{n}} \cos(q)$  has contributions from the mode-dependent tunneling  $J_{\mathbf{n}}$ , the average energy of the transverse mode  $\mathbf{n}$ ,  $\bar{E}_{\mathbf{n}}$ , and the laser detuning  $\delta$ .  $\Omega_{\mathbf{n}}$  is the Rabi frequency for mode  $\mathbf{n}$ . The clock laser with wavelength  $\lambda$  imprints a phase that varies between adjacent lattice sites by  $\phi = \pi\lambda_m/\lambda$ .

If one views the two internal states as a discrete synthetic dimension [40,41], as shown in Fig. 1,  $\hat{H}_{\mathbf{n}}^0$  describes the motion of a charged particle on a two-leg ladder in a magnetic field with flux  $\phi$  per lattice plaquette.  $\hat{H}^0$  hence has the interpretation of many copies of those ladders—one for each transverse mode. By performing a gauge transformation  $\hat{a}_{+,q+\phi,\mathbf{n}} \rightarrow \hat{a}_{+,q,\mathbf{n}}$ ,  $\hat{H}_{\mathbf{n}}^0$  becomes diagonal in momentum space with the excited state dispersion shifted by  $\phi$ ,  $q \rightarrow q + \phi$ . The latter can be then conveniently written in terms of spin-1/2 operators acting on the populated modes

$$\hat{H}^0 = -\sum_{\mathbf{n},q} \mathbf{B}_{\mathbf{n}q} \cdot \hat{\vec{S}}_{\mathbf{n}q}, \quad (3)$$

where  $\mathbf{B}_{\mathbf{n}q} = [\Omega_{\mathbf{n}}, 0, \Delta E_{\mathbf{n}}(q, \phi) + \delta]$ ,  $\Delta E_{\mathbf{n}}(q, \phi) \equiv 2J_{\mathbf{n}}[\cos(q) - \cos(q + \phi)]$ , and  $\hat{S}_{\mathbf{n}q}^{x,y,z}$  are spin-1/2 angular momentum operators. The eigenstates are described by Bloch vectors pointing in the  $xz$  plane, with a direction specified by a single angle  $\theta_{\mathbf{n}q} = \arctan[\Omega_{\mathbf{n}}/[\Delta E_{\mathbf{n}}(q, \phi) + \delta]]$  [see Fig. 2(a)]. The  $q$  dependence of this angle is a manifestation of chiral spin-momentum locking, which is directly connected to the topological chiral edge modes of the two-dimensional Harper-Hofstadter model [41,42].

We first discuss the use of Rabi spectroscopy to probe the noninteracting chiral band structure of Eq. (3). In the regime  $\Omega_0 \ll J_0$ , there exists a finite window of  $\delta$ 's where the two dispersions cross at two special quasimomentum points  $q_n^*$  [see Fig. 2(a)]. The window, whose width is  $8J_n|\sin(\phi/2)|$ , is signaled in the carrier linewidth, and thus when resolved it can be used to determine  $\phi$ . At finite temperature, many transverse modes are populated and

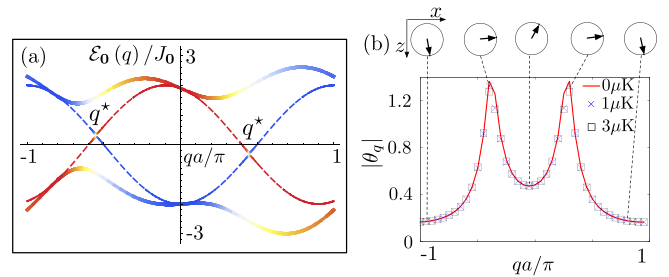


FIG. 2. (a) SOC band structure for  $\delta = -2J_0$ ,  $\Omega_0 = J_0$  (the solid lines) and  $\Omega_0^p = 0.05J_0$  (the dashed lines). The axial depth is  $V = 12$  recoils,  $J_0/h = 42$  Hz, and  $\nu_\perp \approx 900$  Hz. Colors correspond to state character, with  $g$  ( $e$ ) being more blue (red). (b) Chiral Bloch vector angle,  $\theta_{0q}$ , in the  $xz$  plane extracted from Rabi spectroscopy using the protocol explained in the text [39]. The figure shows three temperatures for the parameters of (a).

hence the dependence of  $\Omega_{\mathbf{n}}$  and  $J_{\mathbf{n}}$  on  $\mathbf{n}$  could broaden the line and, in general, prevent an accurate determination of  $\phi$ . However, a direct simulation of the Rabi line shape using the potential Eq. (1) demonstrates that the features of the ideal, zero-temperature line shape are captured even for a temperature of 3  $\mu\text{K}$  [39].

The ability to resolve the  $q_{\mathbf{n}}^*$  resonances that appear across the entire Brillouin zone (BZ) as the detuning is varied can be used to perform momentum-resolved spectroscopy and to precisely determine the chiral Bloch vector angle  $\theta_{0q}$  for given values of  $\Omega_0$  and  $\delta$  from Rabi oscillations. We propose the use of three spectroscopic sequences [39]. One sequence selectively excites atoms at  $q_{\mathbf{n}}^*$  from  $g$  to  $e$  and induces Rabi oscillations. Another filters the dynamics of the excited atoms from the remaining  $g$  atoms, and the third is used to “correct” imperfections arising from finite temperature. As shown in Fig. 2(b), this protocol allows us to extract  $\theta_{0q}$  over the BZ. This method is not restricted to OLCs, requiring only a stable probe, and complements other techniques for measuring band structures [43–45] used in degenerate Fermi gases.

To access the interplay between SOC and interactions, we propose using Ramsey spectroscopy (see Fig. 3). The first pulse rotates the Bloch vector, initially pointing down, by an angle  $\theta_1$ , set by the pulse area, and the second converts the accumulated phase during the dark time  $\tau$  into a  $g - e$  population difference measured as Ramsey fringes. Interactions induce a density-dependent frequency shift in the fringes.

Interactions between two nuclear-spin-polarized atoms depend on the motional and electronic degrees of freedom [23]. When the atoms collide, they experience  $s$ -wave interactions, characterized by the elastic scattering length  $a_{eg}$ , when their electronic state is antisymmetric ( $|eg\rangle - |ge\rangle\rangle/\sqrt{2}$ ). They can also collide via  $p$ -wave interactions, described by the corresponding  $p$ -wave elastic scattering volumes  $b_{gg}^3$ ,  $b_{ee}^3$ , and  $b_{eg}^3$ , in the three possible symmetric electronic configurations  $|gg\rangle$ ,  $|ee\rangle$ , ( $|eg\rangle + |ge\rangle\rangle/\sqrt{2}$ , respectively. In addition to elastic interactions, atoms can also exhibit inelastic collisions. In  $^{87}\text{Sr}$  only the  $ee$  type has been observed to give rise to measurable losses [22,39], while in  $^{173,171}\text{Yb}$ , both  $ee$  and  $eg$  losses have been reported [24,25,36].

When tunneling is suppressed, the differential phase imparted by the laser is irrelevant, and as long as  $\Omega_{\mathbf{n}}$  is

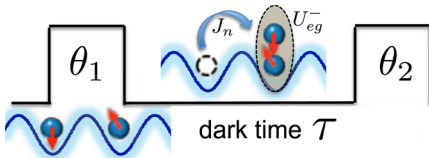


FIG. 3. A clock laser pulse with pulse area  $\theta_1$  imprints a phase difference  $\phi$  between atoms in neighboring sites. Atom tunneling,  $J_{\mathbf{n}}$ , allows for  $s$ -wave interactions,  $\propto U_{eg}^-$ , which are signaled as a density shift in Ramsey spectroscopy after a second pulse of area  $\theta_2$  is applied.

the same for all modes—a condition well satisfied in current OLCs [20]—the collective spin of the atoms within each lattice site remains fully symmetric after the pulse, and only  $p$ -wave collisions occur during the dark time. Measurements under this condition [20,21] indeed observed a frequency shift linearly dependent on the excitation fraction of atoms,  $(1 - \cos \theta_1)/2$ , and fully consistent with a  $p$ -wave interacting model [23]. If instead tunneling is allowed during the dark time, atoms become sensitive to the spatially inhomogeneous spin rotation from the site-dependent laser phase, which in turn allows for  $s$ -wave collisions after a tunneling event (see Fig. 3). The  $s$ -wave collisions in SOC-coupled spin-polarized fermions can lead to exotic phases of matter, including topological quantum liquids [46,47].

In the regime of weak interactions compared to tunneling, we compute the dynamics perturbatively, and we find that SOC manifests itself in the density shift at short times as [39]

$$\Delta\nu = \Delta\nu_0 \left[ 1 + \frac{4\langle J^2 \rangle_{T_R} \tau^2 \zeta \cos \theta_1 \sin^2 \frac{\phi}{2}}{3\hbar^2(C - \chi \cos \theta_1)} \right], \quad (4)$$

where  $\Delta\nu_0 = N(C - \chi \cos \theta_1)$  is the density shift in the absence of tunneling [20,23],  $N$  the mean atom number per pancake,  $\langle J^2 \rangle_{T_R}$  the thermally averaged squared tunneling rate,  $\zeta = (V^{eg} - U^{eg})/2$ ,  $\chi = (V^{ee} + V^{gg} - 2V^{ge})/2$ , and  $C = (V^{ee} - V^{gg})/2$ , with  $V^{aa'} = b_{aa'}^3 \langle P \rangle_{T_R}$  and  $U^{eg} = a_{eg} \langle S \rangle_{T_R}$ . Here,  $\langle P \rangle_{T_R} \propto (T_R)^0$  and  $\langle S \rangle_{T_R} \propto T_R^{-1}$  correspond to the thermal averages of the  $p$ -wave and  $s$ -wave mode overlap coefficients, respectively [23], and  $T_R$  is the radial temperature. For the JILA  $^{87}\text{Sr}$  clock operated at  $T_R \sim (1-5) \mu\text{K}$  and  $\theta_1 \ll \pi$  for  $\tau \sim 80$  ms,  $\Delta\nu_0 \sim -5$  Hz. Since SOC introduces contributions from  $s$ -wave interactions, which can be one order of magnitude larger than  $p$ -wave at  $T_R \sim 1 \mu\text{K}$ , then from Eq. (4) we expect significant modifications of the density shift. In the JILA  $^{87}\text{Sr}$  clock, the ratio of elastic to inelastic  $p$ -wave collision rates has been measured to be  $\sim 2$  under typical conditions [20,22,39], and losses have been compensated for during clock operation by dynamically tracking the population decay during the dark time [20,21]. In Ramsey interrogated SOC systems with dominant  $s$ -wave elastic collisions, inelastic processes are expected to become even less relevant.

The third interrogation protocol we discuss is accomplished by generating a sliding superlattice via a pair of counterpropagating beams close to resonance with the clock transition and with a global phase difference  $\Upsilon(t)$  which can be controlled in time [see Fig. 4(a)]. The noninteracting Hamiltonian, written using a Wannier orbital basis along the lattice direction, is

$$\hat{H}_L^0 = - \sum_{\mathbf{n}, j, a} \left( J_{\mathbf{n}} [\hat{a}_{a, \mathbf{n}, j}^\dagger \hat{a}_{a, \mathbf{n}, j+1} + \text{H.c.}] - \frac{\delta}{2} \alpha \hat{n}_{a, \mathbf{n}, j} \right) - \sum_{\mathbf{n}, j} (\Omega_{\mathbf{n}} \cos[\Upsilon(t) - j\phi] [\hat{a}_{+, \mathbf{n}, j}^\dagger \hat{a}_{-, \mathbf{n}, j} + \text{H.c.}]). \quad (5)$$

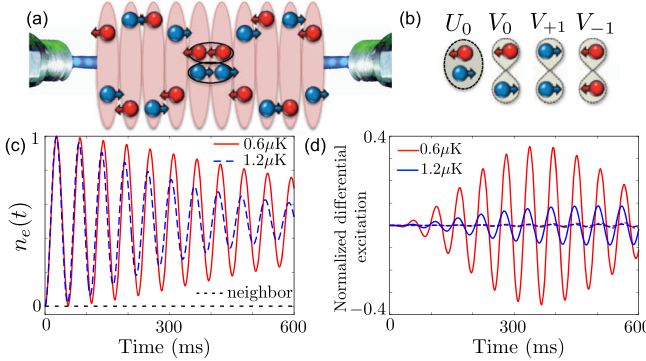


FIG. 4. (a) An additional counterpropagating probing beam with a differential phase  $\Upsilon$  generates a sliding superlattice potential, shown for  $\phi = 7\pi/6$ , corresponding to a  $^{87}\text{Sr}$  OLC. For weak tunneling  $J \ll \Omega$ , transport is energetically suppressed except at resonant defect points (circled). (b) Two-particle interaction sectors classified by the total polarization  $M_x$  and spatial symmetry of the dressed states. An oval (figure eight) denotes a symmetric (antisymmetric) spatial wave function. (c) Dynamics of a single particle at the tunneling resonance for two temperatures (the red solid and blue dashed lines) and an off-resonant site (the black dotted line) for  $J_0/h = 8 \text{ Hz}$ ,  $\Omega_0/h = 1 \text{ kHz}$ ,  $\phi = 7\pi/6$ . (d) Normalized differential excitation extracted as explained in the text with the interaction parameters of Ref. [22]. The  $M_x = 0$  components (the solid lines) involve the  $s$ -wave sector, and thus display a strong dependence of contrast on temperature, while the  $M_{\pm 1}$  sectors (the dashed lines) experience only weaker single-particle thermal dephasing.

As  $\Upsilon(t)$  is changed, the clock laser standing wave “slides” with respect to the optical lattice. This allows for the minimum realization of a topological pump when  $\Upsilon(t)$  is adiabatically varied from  $0 \rightarrow 2\pi$  [28,32–35]. In the weak tunneling limit, the quantized nature of particle transport can be directly linked to spatially isolated tunneling resonances [28]. We now show how those resonances can be spectroscopically measured in OLCs.

Let us first consider the case  $J_n = \delta = 0$  and set  $\phi = 7\pi/6$ , relevant for the  $^{87}\text{Sr}$  system. We write  $\Upsilon = (2\pi s + \Delta\Upsilon)/12$ , with  $0 \leq \Delta\Upsilon < 2\pi$  and  $s$  an integer. Under these conditions, the localized dressed eigenstates are spin polarized along  $\pm x$ , alternating between neighboring sites except for “defects” at  $j_d(r) = 6r + 3 + s$  (with  $r$  being an integer), when  $\cos(\Upsilon - \Delta\Upsilon/12 - j_d\phi) = 0$  and the ground states at  $j_d(r)$  and  $j_d(r) + 1$  point along the same direction. Since tunneling preserves polarization, it is suppressed when  $J_n \ll \Omega_n$  due to the energy offset  $\sim \Omega$  between neighboring sites. The one exception is the case  $\Delta\Upsilon = \pi$ , where the defect pair  $j_d(r)$  and  $j_d(r) + 1$  is resonantly tunnel coupled. Quantized transport occurs when  $\Delta\Upsilon$  is slowly varied across the resonance. Instead of adiabatic transport, we propose spectroscopically resolving the resonance using a Ramsey-type protocol. Here, atoms initially prepared in  $g$  at  $|\delta| \gg \Omega_0$  are adiabatically transferred to the ground dressed state by slowly turning off  $\delta$  at  $\Upsilon = (2\pi s + \Delta\Upsilon_p)/12$ , with  $\Delta\Upsilon_p \neq \pi$ . Then,  $\Upsilon$  is quenched so resonant tunneling is allowed,  $s \rightarrow s + 1$  and

$\Delta\Upsilon = \pi$ , and the system evolves for a time  $\tau$ . Following this evolution, tunneling is turned off and the phase switched back,  $s + 1 \rightarrow s$  and  $\Delta\Upsilon \rightarrow \Delta\Upsilon_p$ . Those atoms which have tunneled at the resonant sites are now in an excited state of the local dressed basis. These excitations can be measured by adiabatically converting the dressed excitations to “bare”  $e$  excitations by adiabatically ramping on  $\delta \gg \Omega_0$ ; this leads to a measurable excited state population  $n_e(t)$ . In Fig. 4(c) we show these tunneling resonances are clearly observable even at finite temperature. Moreover, since resonances are spatially well separated (every six sites), they can be resolved with high, but not necessarily single-site, resolution imaging.

Interactions modify the transport dynamics in this pumping protocol. The sliding superlattice simplifies the treatment of interactions by isolating resonant site pairs  $\{j_d, j_d + 1\}$ . We consider the case where at most two atoms occupy the resonant sites, a condition which can be achieved by decreasing the atomic density with a large-volume dipole trap [16]. The two-particle states can be classified in terms of the atoms’ spin polarization along  $x$  in four sectors: three symmetric ones (triplets) with total  $x$  polarization  $M_x = +1, -1, 0$  and an  $M_x = 0$  singlet. Within each sector, the dressed states’ interaction parameters are given by [39]  $V_{+1} = V_{-1} = (V^{gg} + V^{ee} + 2V^{eg})/4$ ,  $V_0 = (V^{gg} + V^{ee})/2$ , and  $U_0 = U^{eg}$  [see Fig. 4(b)]. Since the  $p$ -wave parameters are not SU(2) symmetric, i.e.,  $b_{ee} \neq b_{gg} \neq b_{eg}$ , the triplet sectors are coupled. However, in the weakly interacting limit  $V^{ab} \ll \Omega$ , the triplets are separated by energy gaps  $\sim \Omega$  and coupling between the sectors can be neglected. The singlet sector is always decoupled from the triplets.

Within each sector, interactions modify the dynamics, making it sensitive to temperature and density. The modifications can be extracted by performing measurements of the atom number-normalized excitation fraction for different densities and then differentiating the high-density and low-density results [39]. This procedure removes the single-particle contribution and is particularly suitable for characterizing the role of interactions in clock experiments [20,22]. The normalized differential excitation is shown in Fig. 4(d). For the adiabatic dressed state preparation, all four manifolds, and hence all interaction parameters  $V_{\pm,0}$ ,  $U_0$ , contribute to the dynamics. A filtering protocol that uses the  $ee$  losses can be used to separate the dynamics of the various sectors. For example, by transferring all atoms to the  $e$  state and holding before the adiabatic ground state preparation, the doubly occupied  $M_x = \pm 1$  triplet sectors will be removed and only the  $M_x = 0$  singlet and triplet remain and contribute (here, the ground dressed states have one atom at  $j_d$  and  $j_d + 1$ ). As shown in Fig. 4, the dynamics of the  $V_{\pm,0}$  and  $U_0$  sectors can be distinguished by the different scaling of the  $p$ - and  $s$ -wave interaction parameters with temperature  $T_R$ ,  $V_{\pm,0}(T_R) \sim \text{const}$ , and  $U_0(T_R) \sim T_R^{-1}$  [23] [see Fig. 4(d)]. By comparing these dynamics to that without the holding

time, information about the  $M_x = \pm 1$  dynamics can be extracted. In general,  $s$ -wave interactions, purely elastic for nuclear-spin-polarized Sr, dominate the normalized differential contrast, with  $p$ -wave contributions (including losses) relevant only at hotter temperatures.

*Summary.*—We have described approaches for implementing and probing SOC and its interplay with  $s$ - and  $p$ -wave interactions in OLCs. These open the unique opportunity of exploring, for the first time, a controllable interplay of interactions, spin-orbit coupling, and nontrivial topology in regimes where a complete theoretical treatment can also be performed. While the described protocols work at the temperatures achievable in current OLCs, their sensitivity and applicability are expected to significantly improve when we operate the clock in the quantum degenerate regime. Moreover, if nuclear spins are included, they can open a window for the investigation of SOC with  $SU(N)$ -symmetric collisions [48].

We thank Ed Marti and James Thompson for their comments on the manuscript, and Leonid Isaev and the JILA Sr clock team for discussions. This work was supported by the NSF (Grants No. PIF-1211914 and No. PFC-1125844), AFOSR, AFOSR-MURI, NIST and ARO, EPSRC Grant No. EP/K030094/1, and the JILA Visiting Fellows Program. M. L. W. thanks the NRC postdoctoral fellowship program for support. A. K. was supported by the U.S. Department of Defense through the NDSEG program.

\*Corresponding author.

mwall.physics@gmail.com

<sup>†</sup>Present address: International Center for Quantum Materials, School of Physics, Peking University, Beijing 100871, China.

- [1] V. Galitski and I. B. Spielman, Spin-orbit coupling in quantum gases, *Nature (London)* **494**, 49 (2013).
- [2] N. R. Cooper, in Many-Body Physics with Ultracold Gases, *Proceedings of the Les Houches Summer School, Session 94*, edited by C. Salomon, G. V. Shlyapnikov, and L. F. Cugliandolo (Oxford University Press, Oxford, 2013).
- [3] J. Dalibard, F. Gerbier, G. Juzeliūnas, and P. Öhberg, Colloquium: Artificial gauge potentials for neutral atoms, *Rev. Mod. Phys.* **83**, 1523 (2011).
- [4] N. Goldman, G. Juzeliūnas, P. Ohberg, and I. B. Spielman, Light-induced gauge fields for ultracold atoms, *Rep. Prog. Phys.* **77**, 126401 (2014).
- [5] H. Zhai, Degenerate quantum gases with spin-orbit coupling: A review, *Rep. Prog. Phys.* **78**, 026001 (2015).
- [6] B. K. Stuhl, H.-I. Lu, L. M. Aycock, D. Genkina, and I. B. Spielman, Visualizing edge states with an atomic Bose gas in the quantum Hall regime, *Science* **349**, 1514 (2015).
- [7] M. Mancini, G. Pagano, G. Cappellini, L. Livi, M. Rider, J. Catani, C. Sias, P. Zoller, M. Inguscio, M. Dalmonte, and L. Fallani, Observation of chiral edge states with neutral fermions in synthetic Hall ribbons, *Science* **349**, 1510 (2015).

- [8] X. Cui, B. Lian, T.L. Ho, B. Lev, and H. Zhai, Synthetic gauge field with highly magnetic lanthanide atoms, *Phys. Rev. A* **88**, 011601(R) (2013).
- [9] F. Gerbier and J. Dalibard, Gauge fields for ultracold atoms in optical superlattices, *New J. Phys.* **12**, 033007 (2010).
- [10] J. Ruostekoski, G. V. Dunne, and J. Javanainen, Particle Number Fractionalization of an Atomic Fermi-Dirac Gas in an Optical Lattice, *Phys. Rev. Lett.* **88**, 180401 (2002).
- [11] J. Ruostekoski, J. Javanainen, and G. V. Dunne, Manipulating atoms in an optical lattice: Fractional fermion number and its optical quantum measurement, *Phys. Rev. A* **77**, 013603 (2008).
- [12] Andrew J. Daley, Martin M. Boyd, Jun Ye, and Peter Zoller, Quantum Computing with Alkaline-Earth-Metal Atoms, *Phys. Rev. Lett.* **101**, 170504 (2008).
- [13] A. V. Gorshkov, A. M. Rey, A. J. Daley, M. M. Boyd, J. Ye, P. Zoller, and M. D. Lukin, Alkaline-Earth-Metal Atoms as Few-Qubit Quantum Registers, *Phys. Rev. Lett.* **102**, 110503 (2009).
- [14] A. D. Ludlow, M. M. Boyd, J. Ye, E. Peik, and P. O. Schmidt, Optical atomic clocks, *Rev. Mod. Phys.* **87**, 637 (2015).
- [15] M. M. Boyd, T. Zelevinsky, A. D. Ludlow, S. M. Foreman, S. Blatt, T. Ido, and J. Ye, Optical atomic coherence at the 1-second time scale, *Science* **314**, 1430 (2006).
- [16] B. J. Bloom, T. L. Nicholson, J. R. Williams, S. L. Campbell, M. Bishop, X. Zhang, W. Zhang, S. L. Bromley, and J. Ye, An optical lattice clock with accuracy and stability at the  $10^{-18}$  level, *Nature (London)* **506**, 71 (2014).
- [17] T. L. Nicholson *et al.*, Systematic evaluation of an atomic clock at  $2 \times 10^{-18}$  total uncertainty, *Nat. Commun.* **6**, 6896 (2015).
- [18] N. Hinkley, J. A. Sherman, N. B. Phillips, M. Schioppo, N. D. Lemke, K. Belyov, M. Pizzocaro, C. W. Oates, and A. D. Ludlow, An atomic clock with  $10^{-18}$  instability *Science* **341**, 1215 (2013).
- [19] U. Ichiro, M. Takamoto, M. Das, T. Ohkubo, and H. Katori, Cryogenic optical lattice clocks, *Nat. Photonics* **9**, 185 (2015).
- [20] M. J. Martin, M. Bishop, M. D. Swallows, X. Zhang, C. Benko, J. von Stecher, A. V. Gorshkov, A. M. Rey, and J. Ye, A quantum many-body spin system in an optical lattice clock, *Science* **341**, 632 (2013).
- [21] N. D. Lemke, J. von Stecher, J. A. Sherman, A. M. Rey, C. W. Oates, and A. D. Ludlow,  $p$ -Wave Cold Collisions in an Optical Lattice Clock, *Phys. Rev. Lett.* **107**, 103902 (2011).
- [22] X. Zhang, M. Bishop, S. L. Bromley, C. V. Kraus, M. S. Safronova, P. Zoller, A. M. Rey, and J. Ye, Spectroscopic observation of  $SU(N)$ -symmetric interactions in Sr orbital magnetism, *Science* **345**, 1467 (2014).
- [23] A. M. Rey, A. V. Gorshkov, C. V. Kraus, M. J. Martin, M. Bishop, M. D. Swallows, X. Zhang, C. Benko, J. Ye, N. D. Lemke, and A. D. Ludlow, Probing many-body interactions in an optical lattice clock, *Ann. Phys. (Amsterdam)* **340**, 311 (2014).
- [24] M. Bishop, M. J. Martin, M. D. Swallows, C. Benko, Y. Lin, G. Quéméner, A. M. Rey, and J. Ye, Inelastic collisions and density-dependent excitation suppression in a  $^{87}\text{Sr}$  optical lattice clock, *Phys. Rev. A* **84**, 052716 (2011).
- [25] A. D. Ludlow, N. D. Lemke, J. A. Sherman, C. W. Oates, G. Quéméner, J. von Stecher, and A. M. Rey, Cold-collision-shift cancellation and inelastic scattering in a Yb optical lattice clock, *Phys. Rev. A* **84**, 052724 (2011).

- [26] R. A. Williams, L. J. LeBlanc, K. Jiménez-García, M. C. Beeler, A. R. Perry, W. D. Phillips, and I. B. Spielman, Synthetic partial waves in ultracold atomic collisions, *Science* **335**, 314 (2012).
- [27] Z. Fu, L. Huang, Z. Meng, P. Wang, L. Zhang, S. Zhang, H. Zhai, P. Zhang, and J. Zhang, Production of Feshbach molecules induced by spin-orbit coupling in Fermi gases, *Nat. Phys.* **10**, 110 (2014).
- [28] N. R. Cooper and A. M. Rey, Adiabatic control of atomic dressed states for transport and sensing, *Phys. Rev. A* **92**, 021401(R) (2015).
- [29] Michael Lohse, Christian Schweizer, Oded Zilberberg, Monika Aidelsburger, and Immanuel Bloch, A Thouless quantum pump with ultracold bosonic atoms in an optical superlattice, *Nat. Phys.*, doi:10.1038/nphys3584 (2015).
- [30] Shuta Nakajima, Takafumi Tomita, Shintaro Taie, Tomohiro Ichinose, Hideki Ozawa, Lei Wang, Matthias Troyer, and Yoshiro Takahashi, Topological Thouless pumping of ultracold fermions, arXiv:1507.02223.
- [31] Hsin-I Lu *et al.*, Geometrical pumping with a Bose-Einstein condensate, arXiv:1508.04480.
- [32] D. J. Thouless, Quantization of particle transport, *Phys. Rev. B* **27**, 6083 (1983).
- [33] Lei Wang, Matthias Troyer, and Xi Dai, Topological Charge Pumping in a One-Dimensional Optical Lattice, *Phys. Rev. Lett.* **111**, 026802 (2013).
- [34] Feng Mei, J.-B. You, D.-W. Zhang, X. C. Yang, R. Fazio, S.-L. Zhu, and L.C. Kwek, Topological insulator and particle pumping in a one-dimensional shaken optical lattice, *Phys. Rev. A* **90**, 063638 (2014).
- [35] R. Wei and E. J. Mueller, Anomalous charge pumping in a one-dimensional optical superlattice, *Phys. Rev. A* **92**, 013609 (2015).
- [36] F. Scazza, C. Hofrichter, M. Höfer, P. C. De Groot, I. Bloch, and S. Fölling, Observation of two-orbital spin-exchange interactions with ultracold SU( $N$ )-symmetric fermions, *Nat. Phys.* **10**, 779 (2014).
- [37] G. Cappellini *et al.*, Direct Observation of Coherent Interorbital Spin-Exchange Dynamics, *Phys. Rev. Lett.* **113**, 120402 (2014).
- [38] M. L. Wall, K. R. A. Hazzard, and A. Maria Rey, Effective many-body parameters for atoms in nonseparable Gaussian optical potentials, *Phys. Rev. A* **92**, 013610 (2015).
- [39] See Supplemental Material at <http://link.aps.org/supplemental/10.1103/PhysRevLett.116.035301> for a derivation of the density shift in Ramsey spectroscopy, the extraction of the chiral Bloch vector angle in Rabi spectroscopy, and the interaction-induced contrast decay with the sliding clock superlattice.
- [40] A. Celi, P. Massignan, J. Ruseckas, N. Goldman, I. B. Spielman, G. Juzeliūnas, and M. Lewenstein, Synthetic gauge fields in synthetic dimensions, *Phys. Rev. Lett.* **112**, 043001 (2014).
- [41] D. Hügel and B. Paredes, Chiral ladders and the edges of Chern insulators, *Phys. Rev. A* **89**, 023619 (2014).
- [42] Y. Hatsugai, Topological aspects of the quantum Hall effect, *J. Phys. Condens. Matter* **9**, 2507 (1997).
- [43] L. Tarruell, D. Greif, T. Uehlinger, G. Jotzu, and T. Esslinger, Creating, moving and merging Dirac points with a Fermi gas in a tunable honeycomb lattice, *Nature (London)* **483**, 302 (2012).
- [44] M. Atala, M. Aidelsburger, J. T. Barreiro, D. Abanin, T. Kitagawa, E. Demler, and I. Bloch, Direct measurement of the Zak phase in topological Bloch bands, *Nat. Phys.* **9**, 795 (2013).
- [45] L. Duca, T. Li, M. Reitter, I. Bloch, M. Schleier-Smith, and U. Schneider, An Aharonov-Bohm interferometer for determining Bloch band topology, *Science* **347**, 288 (2015).
- [46] C. Zhang, S. Tewari, R. M. Lutchyn, and S. Das Sarma,  $p_x + ip_y$  Superfluid from *s*-Wave Interactions of Fermionic Cold Atoms, *Phys. Rev. Lett.* **101**, 160401 (2008).
- [47] B. Juliá-Díaz, T. Graß, O. Dutta, D. E. Chang, and M. Lewenstein, Engineering *p*-wave interactions in ultracold atoms using nanoplasmonic traps, *Nat. Commun.* **4**, 2046 (2013).
- [48] M. Cazalilla and A. M. Rey, Ultracold Fermi gases with emergent SU( $N$ ) Symmetry, *Rep. Prog. Phys.* **77**, 124401 (2014).